14

STATE RESEARCH CENTER OF RUSSIA
Institute of Theoretical
and Experimental Physics

FERMILAB 17-97
SEP 4 1997
LIBRARY

L.G. Vorobiev

A Method for Aspherical Lenses Design Applicable to Charged Particles and Light Optics Optimization

ITEP-17-97
Fermilab Library
0 1160 0057979 1

Moscow 1997

UDK 621.384 M-16

A METHOD FOR ASPHERICAL LENSES DESIGN APPLICABLE TO CHARGED PARTICLES AND LIGHT OPTICS OPTIMIZATION; Preprint ITEP 17-97/

L.G.Vorobiev - M., 1997 - 16p.

Optimal surfaces of non-spherical lenses with upgraded optical characteristics were found as a solution of a constrained variational problem. The applications of the developed numerical approach could be found in mechanics, charged particles and light optics design.

Fig. - 12, ref. - 7 name.

© Институт теоретической и экспериментальной физики, 1997

[1]e-mail: lgvor@vxitep.itep.ru

1 Introduction

Spherical lenses are widely used in light optics and have those advantages, that the fabrication and control of spherical surfaces are rather easy to provide. Another circumstance, which facilitate a theoretical analysis and practical design of optical systems, is that high order aberrations for these lenses are expressed by the same universal formulae. However, some imperfections of spherical lenses are inevitable and deteriorate the quality of focussing especially when using non-paraxial large aperture ratio and/or inclined off-axis beams. As a result, well-known aberrations arise, such as astigmatism, coma, spherical aberrations, distortions and field curvature [1, 2].

A possible way to improve parameters of optical devices is to use aspherical lenses. Application of these lenses becomes very important, if we want to build optical objectives with large relative and angular apertures, with increased brightness, sharpness and extreme resolving power. Best brands of photocameras, available now on the market, use aspherical high-performance

lenses. Meantime, the idea to use non-spherical glass surfaces originates from Descartes and Huygens [3], who had studied some features of aspherical lenses and derived formulae for their surfaces.

Nowadays, the optimization of optical systems uses widely computer methods. A search of optimal surface of a lense can be formulated as a solution of a variational problem:

$$\Phi(\mathrm{F}(s)) \to \min \tag{1}$$

subject to:

$$\mathrm{F}^{(p)}(\tilde{s}_0) = \mathcal{F}_0^{(p)} \quad \mathrm{F}^{(p)}(\tilde{s}_1) = \mathcal{F}_1^{(p)} \quad p = 0, 1, \ldots P \tag{2}$$

where the functional $\Phi(\mathrm{F})$ expresses a quantitative criterion of optimization and the unknown function $\mathrm{F}(s)$ can vary within an interval $[\tilde{s}_0, \tilde{s}_1]$ ($\tilde{s} = \tilde{s}_1 - \tilde{s}_0$ is its length); $\mathrm{F}^p = d^p\mathrm{F}/ds^p$ and P stands for the number of constraints. The set of conditions (2) defines the function and its higher derivatives on the boundary (the specific construction of the functional $\Phi(\mathrm{F})$, which estimates the quality of focussing, and corresponding boundary constraints will be considered in section 2).

In the paper [4] we developed a "shaping algorithm" to find the optimal solution $\mathrm{F}^{opt}(s)$ of the problem (1)-(2)), providing min $\Phi(\mathrm{F})$. Numerical experiments demonstrated an efficiency of that method for mechanics and charged particle optics [4] and in this paper we try to systematize and broaden application of this algorithm for light optics.

In section 2 aspherical lenses with improved optical characteristics will be designed, when their shape will be found as a solution of the problem (1)-(2). The optimization will allow to suppress spherical and other high-order aberrations and may help to reduce a number of lenses, installed in optical objectives. In addition, in section 3 we develop further the computational scheme of the "shaping algorithm".

2 Design of Aspherical Lenses

Basic physical formulae. In this paper we restrict ourselves by considerations of monochromatic light beams, omitting the wave nature of the light. Optimal surfaces of lenses will be found purely in frames of geometrical ray optics, based on the Fermat's principle of least time. The physical model, realized in the block of ray tracing, uses only the refraction law, which gives a relation between the angle of incidence γ_1 and the angle of refraction γ_2 as the following:

$$\frac{\sin\gamma_1}{\sin\gamma_2} = n_{21}$$

where the coefficient n_{21} stands for the refraction factor (as is well known, $n_{21} \geq 1$ and $n_{21} = 1$ for vacuum; for glass lenses this coefficient is about $n_{21} \approx 1.5 - 1.65$). When a lense thickness is relatively small in comparison with its size, there is a relation between the image distance $\mathbf{L}^{image}$ and the object distance $\mathbf{L}^{object}$:

$$\frac{1}{\mathbf{L}^{image} - D_1} - \frac{1}{\mathbf{L}^{object} - D_2} = (n_{21} - 1)(\frac{1}{R_1} - \frac{1}{R_2}) \tag{3}$$

where $R_{1,2}$ are curvature radii and $D_{1,2}$ are thicknesses of the lense from the corresponding surfaces to the center. The validity of the equation (3) takes place when $D_{1,2} \ll |R_{1,2}|$ and all rays are paraxial. This model is the so-called "thin lense approximation".

Let us consider an example. We take a symmetrical spherical lense (with both radii $|R_{1,2}| = 5$), whose surfaces are described by the shape function $\mathrm{F}_{sph}(s)$, as the following:

$$x^2 + (y \pm 4)^2 = R_{1,2}^2$$

Substituting in the formula (3) $R_1 = 5,\ R_2 = -5,\ \mathbf{L}^{object} = 10,\ D_{1,2} = 1$ and assuming the refraction factor $n_{21} = 1.50$ (such a magnitude is close to a refraction factor of a usual glass), we find that image distance must be equal to $\mathbf{L}^{image} = -12.25$.

For numerical simulation let us consider N^{rays} rays, ejected from the object point $(0, \mathbf{L}^{image})$ with different angles. Firstly we consider a narrow beam (all rays are paraxial), focused by a spherical lense with the shape function $\mathrm{F}_{sph}(s)$. As shown in Fig. 1, all paraxial rays have a fine focus in the point $\mathbf{L}^{image} = -12.23$, that coincides pretty well with analytical result. [2]

When we use non-paraxial rays, the quality of focussing will be spoiled, as shown in Fig. 2, that illustrates the well known effect of spherical aberrations, relevant to any spherical lense. For the focusing regime, using the full aperture, the dilution in the focus will be even worse.

Optimal "shaping" of lense surfaces. Now we apply the "shaping algorithm" [4] to find aspherical lenses with improved quality of focussing. Let

[2]The image distance $\mathbf{L}^{image} = -12.23$ is a precise result of numerical simulation, based on the refraction law. The abovementioned analytical formula for a thin lense (3) gives only approximate result.

us consider N^{rays} rays, ejected from the object point $(0, \mathrm{L}^{image})$ with different angles. The current coordinate and slope of every ray are given by $x_r(l), x'_r(l)$ with l is a current distance from the object point. The most natural and simple construction of optimization criterion is a minimum of rms deviation from the image point:

$$\Phi(\mathrm{F}) = \Delta(F) = \frac{1}{N^{rays}} \left\{ \sum_{r=1}^{N^{rays}} x_r^2(\mathrm{L}^{image}) \right\}^{1/2} \to \min \tag{4}$$

The minimal possible value of Φ is zero, that corresponds to ideal focussing without dilution.

Fig. 3 shows the shape function $\mathrm{F}_{sph}(s)$ of a usual spherical glass lense in comparison with the shape function $\mathrm{F}_{opt1}(s)$, corresponding to the optimized aspherical lense. The shaping algorithm finds the optimal surfaces for various combinations of constraints (the central thickness and boundary derivatives) and for desirable object and image distances. In Fig. 4 the profiles of the optimal shape functions $\mathrm{F}_{opt1}(s)$, $\mathrm{F}_{opts}(s)$ are plotted and Figs. 5,6 show the optimized focusing regimes with small focusing spots for $|\mathrm{L}^{image}| = 15$ and 10. The pictures with reduced image distance $|\mathrm{L}^{image}| = 5$ are demonstrated in Figs. 7,8 and again we obtain a fine focussing. The corresponding shape functions are shown in Fig. 9. Note, that $\mathrm{F}_{opt4}(s)$ has a rather complicated profile, that was a result of specific boundary limitations, assigned as an initial data for the "shaping algorithm".

Distortion. The next question, which arise after suppressing the spherical aberration is a minimization of distortion. If the object has a height h^{object} and the image has correspondingly h^{image}, then the presence of distortion means a changing of magnification factor K for different "h" magnitudes.

$$K(\mathrm{F}) = \frac{h^{object}}{h^{image}}$$

And the distortion will be absent when $K(\mathrm{F}) \equiv const$. The suppression of distortion is important, when we wish to obtain the true image picture for the full aperture.

A possible way to estimate the change of $K(\mathrm{F})$ numerically is to compute the rms deviation

$$\delta = \frac{1}{N^{rays}} \left\{ \sum_{r=1}^{N^{rays}} \left[\frac{x_r(\mathrm{L}^{object} + l^{object})}{x_r(\mathrm{L}^{image} + l^{image})} - \frac{x_1(\mathrm{L}^{object} + l^{object})}{x_1(\mathrm{L}^{image} + l^{image})} \right]^2 \right\}^{1/2}$$

where the object is shifted from focus coordinate by the distance l^{object} and image has a corresponding shift l^{image} from the image point.

Obviously, for $\delta = 0$ we have no distortion at all. If we want to obtain a true image picture and maintain the fine focussing, then the minimization of Δ from Eqs. 4 should be combined with $\min \delta$. Therefore, the construction of the functional $\Phi(F)$ from (4) should include an additional "distortion term":

$$\Phi(\mathrm{F}) = \Delta + \delta \to \min \tag{5}$$

In the Fig. 12 one can see the distortion factor for various shape functions $\mathrm{F}_{opt3}(s)$ and $\mathrm{F}^*_{opt3}(s)$. For optimal shape function $\mathrm{F}^*_{opt3}(s)$ the behaviour of $K(\mathrm{F})$ is practically constant for the full aperture range. Note, that the both functions are rather close as plotted in Fig. 11 that assumes a high precision in fabrication of such lenses. To maintain the distortion-free focussing for wide ranges of the image points requires additional studies.

We could see, how one optimized lense managed with spherical aberrations and distortion for non-paraxial beams, using the full aperture. Meanwhile, the other optical imperfections, relevant to off-axis effects, the focussing of inclined beams and those, which deal with the wave nature of the light (e.g. chromatic aberrations), could be suppressed using two or even more lenses with different refraction factors. The construction of $\Phi(\mathrm{F})$ will include new summands, responsible for corresponding imperfections. Technically the work of the shaping algorithm, which minimize the functional $\Phi(\mathrm{F})$, will not be changed, however, the convergence of the minimization procedure may be slower. This is why in the next section we pay attention to possible modification of the method to speed up the convergence to the optimal solution.

3 Numerical Method

A detailed computational scheme of the "shaping algorithm" to solve the constrained variational problem (1)–(2) was described in the paper [4]. We make now minor changes in the computational scheme, which however could increase the flexibility of optimization and upgrade the convergence of the minimization process. For sake of brevity let us consider only the function values and its derivatives on the boundary. For higher derivatives the computational scheme can be easy generalized.

The shape function can be splitted as $\mathrm{F}(s) = \mathrm{F}_{var}(s) + \mathrm{F}_{fix}(s)$ where the summands satisfy correspondingly

$$\begin{cases} \mathrm{F}_{var}(\tilde{s}_0) = \mathcal{F}_0 & \mathrm{F}_{var}(\tilde{s}_1) = \mathcal{F}_1 \\ \mathrm{F}'_{var}(\tilde{s}_0) = 0 & \mathrm{F}'_{var}(\tilde{s}_1) = 0 \end{cases} \tag{6}$$

and

$$\begin{cases} \mathrm{F}_{fix}(\tilde{\mathrm{s}}_0) = 0 & \mathrm{F}_{fix}(\tilde{\mathrm{s}}_1) = 0 \\ \mathrm{F}'_{fix}(\tilde{\mathrm{s}}_0) = \mathcal{F}'_0 & \mathrm{F}'_{fix}(\tilde{\mathrm{s}}_1) = \mathcal{F}'_1 \end{cases} \tag{7}$$

Such a representation allows to formulate an auxiliary optimization problem (1) subject to (6)-(7), where the function $F_{var}(s)$ will vary and the function $F_{fix}(s)$ will not change during the optimization. In this new formulation we should find only the solution of (1) with boundary constraints (6).

As it was shown in the papers [5, 6], this solution F_1^{opt} may be found via Fourier representation, as the following

$$\mathrm{F}_{var}(s) = f_0 + \sum_{k=1}^{m} f_k \cos(k\pi(s - \tilde{\mathrm{s}}_0)/\tilde{\mathrm{s}}) \tag{8}$$

with $\{f_k\}$ satisfying to

$$\begin{cases} f_0 + f_1 + f_2 + \ldots + f_m = \mathcal{F}_0 \\ f_0 - f_1 + f_2 - \ldots + (-1)^m \cdot f_m = \mathcal{F}_1 \end{cases} \tag{9}$$

A search for the optimal function F_{var}^{opt} was reduced to a minimization of $\Phi(\mathrm{F}_{var})$ subject to (9). To find the optimal vector $\vec{f}^{\,opt}$ we used a step by step descent gradient minimization procedure:

$$\vec{f}^{\,n+1} = \vec{f}^{\,n} - \delta \cdot \vec{g}_P \tag{10}$$

where δ corresponds to $\min\ \Phi(\vec{f}^{\,n+1}(\delta))$ and $\vec{g}_P$ stands for a gradient projection $\vec{g} = grad\ \Phi(\vec{f}^{\,n})$ onto the hyperplane "P", described by (9). The validity of the boundary constraints of this minimization procedure are being maintained automatically and the function F_{fix} satisfies (7), since it is fixed by definition. When finding the vector $\vec{f}^{\,opt}$ we get immediately $\mathrm{F}_{var}^{opt}(s)$ and the corresponding solution F_{opt} of the general variational problem (1)–(2).

The splitting of the original shape function $\mathrm{F}(s)$ occurs to be helpful from the point of view acceleration of the convergence. We could observe during the numerical experiments, that even functions (cosine functions) in the representation (8) allow to speed up the convergence of minimization for some specific foundary limitations. The absence of odd functions, such as sinus, allows to use rather a short Fourier expansion and make the whole procedure more flexible. As the F_{fix} function in particular cases we can choose, for example, a cubic interpolation.

4 Discussion

The introduced algorithm was applied to find the optimal shape of a single lense. We emphasize, that the found aspherical surfaces were found numerically and their family is more general, than second order analytical functions (e.g. hyperbolical, elliptical etc.). When increasing the number of harmonics in Fourier representation, we can approximate very special functions, moreover, we can even manage with infinite boundary derivatives, as it was shown in [4].

Beside that, there are no limitations to generalize our approach to multi-lenses systems and/or multi-layers lenses design; the optimization may be performed also for lenses with different refraction fartors to minimize the dispersion of the light. The construction of the optimization criterion Φ will correspond to the desireable optical regime and will include the terms, responsible for the particular optical effects, as we could see above; it can include also the factor of weight and costs. This last circumstance might be important for compact cameras.

In comparison with charged particles optics we have that advantage, that computations for rays tracing are very fast and straightforward. We are not really limited in using a big number of rays in light beams and the most time-consumed block in our program is the "shaping algorithm" itself. Simulations of charged particles propogation through the spacial electromagnetic fields takes much more time. The particles tracing should be combined the fast Laplace solver and uses the motion equations integrator (if the space charge effects are negligible, it could be the Runge-Kutta 4-th order integrator). As a result, the optimal shaping of electrodes for charged particle optics, requires rather powerful computational capacities. Nevertheless, as it was demonstrated in [4, 5, 6] the optimal shape of electrodes for axially symmetrical cases could be done within a reasonable time.

Acknowledgements

The author wants to thank Dr. R.W.Müller (GSI, Darmstadt, Germany), who originally drew his attention to the application of the shaping algorithm to the light optics optimization and for useful comments.

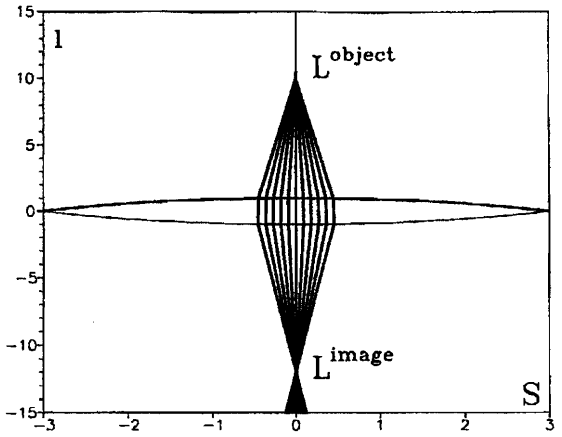

Figure 1: Paraxial rays $x_r(l)$ (r=1,...,10) passing through a spherical lense with the shape function $F_{sph}(s)$. The object distance is $L^{object} = 10$ and the image distance is $L^{image} = -12.2$ (here and below the axes units are dimensionless). The focusing spot is small.

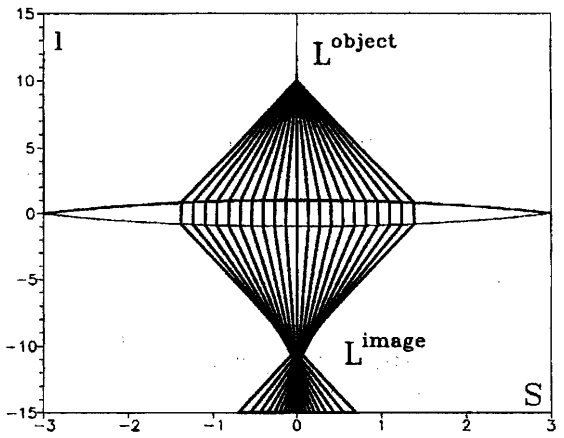

Figure 2: Non-paraxial rays $x_r(l)$ (r=1,...,20), passing a spherical lense with the shape function $F_{sph}(s)$. The object distance is equal $L^{object} = 10$, and the image focusing spot is diluted.

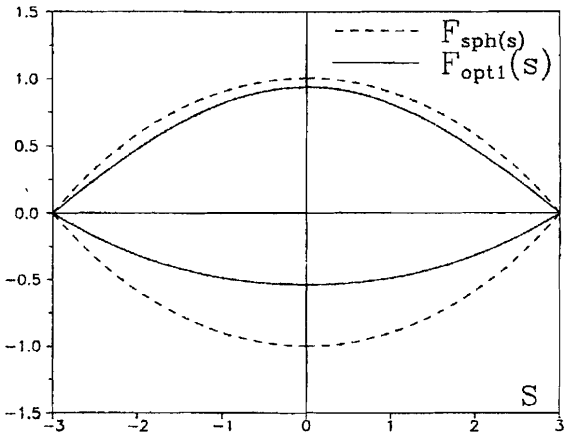

Figure 3: Shape functions $F_{sph}(s)$ and $F_{opt1}(s)$.

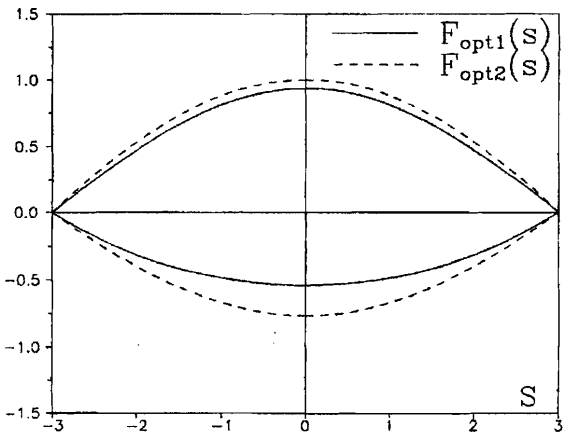

Figure 4: Shape functions $F_{opt1}(s)$, $F_{opt2}(s)$ for optimized lenses.

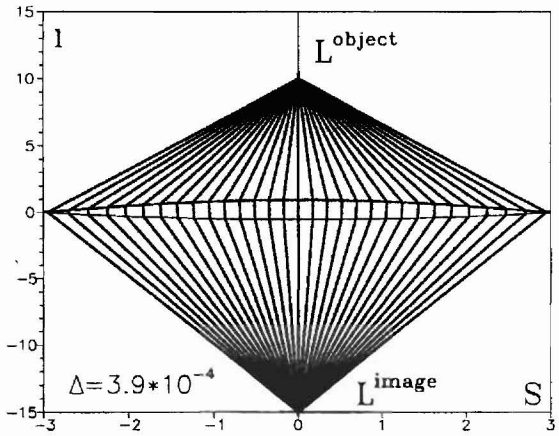

Figure 5: Non-paraxial rays (the full aperture is used) through an optimized lense with profile $F_{opt1}(s)$, providing a fine focussing. The object distance is $L^{object} = 10$ and the image distance is $L^{image} = -15$ (units are dimensionless).

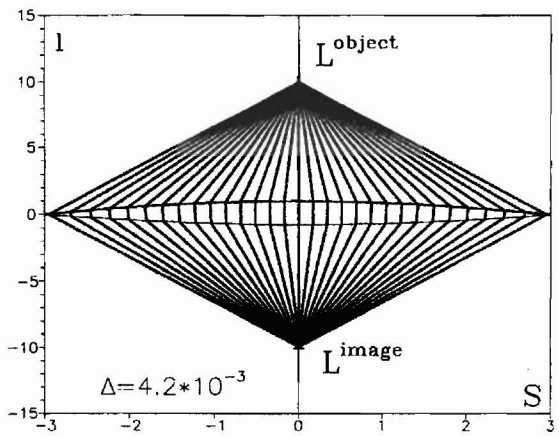

Figure 6: Non-paraxial rays (the full aperture is used) through an optimized lense with profile $F_{opt2}(s)$, providing a fine focussing. The object distance is $L^{object} = 10$ and the image distance is $L^{image} = -10$.

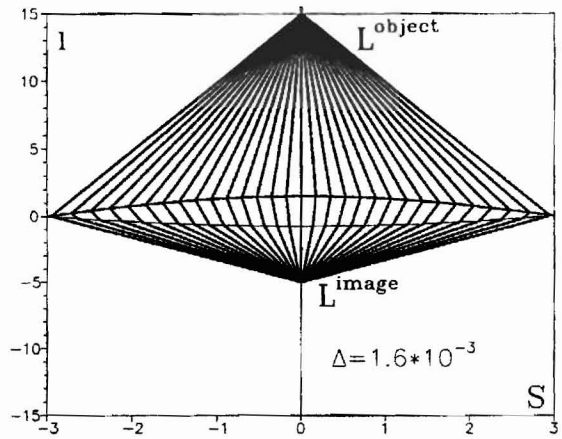

Figure 7: Non-paraxial rays (the full aperture is used) through an optimized lense with profile $F_{opt3}(s)$, providing a fine focussing. The object distance is $\mathbf{L}^{object} = 15$ and the image distance is $\mathbf{L}^{image} = -5$.

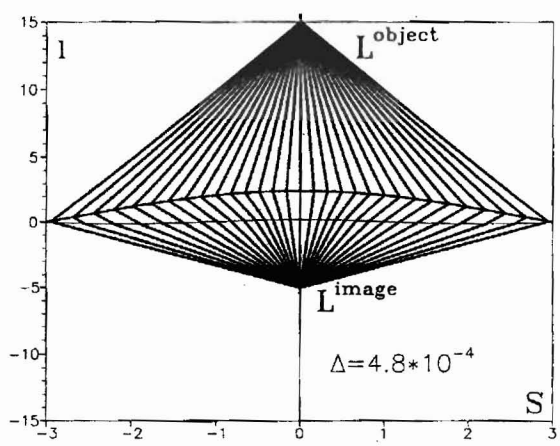

Figure 8: Non-paraxial rays (the full aperture is used) through an optimized lense with profile $F_{opt4}(s)$, providing a fine focussing. The object distance is $\mathbf{L}^{object} = 15$ and the image distance is $\mathbf{L}^{image} = -5$.

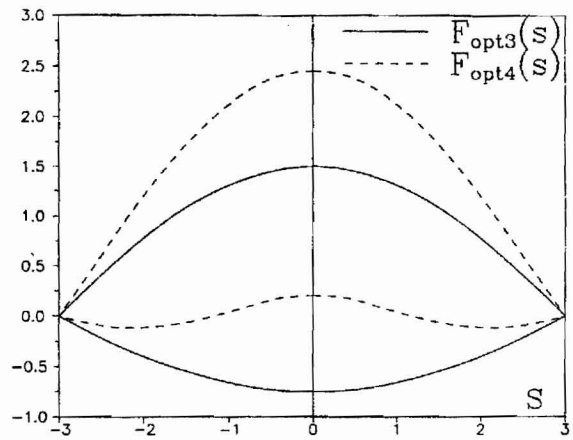

Figure 9: Shape functions $F_{opt3}(s)$, $F_{opt4}(s)$.

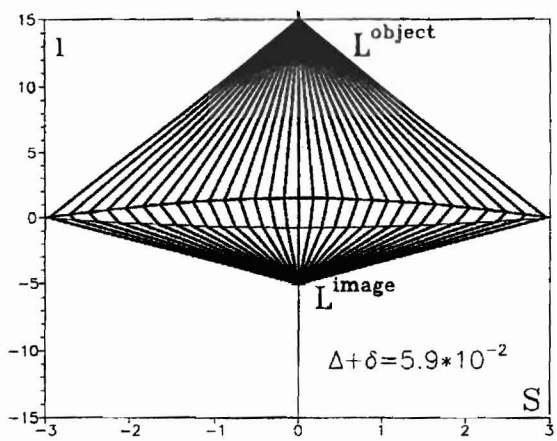

Figure 10: Non-paraxial rays through an optimized lense with profile $F^*_{opt3}(s)$, providing a fine focussing and reduced distortion for the full aperture. The object distance is $L^{object} = 15$ and the image distance is $L^{image} = -5$.

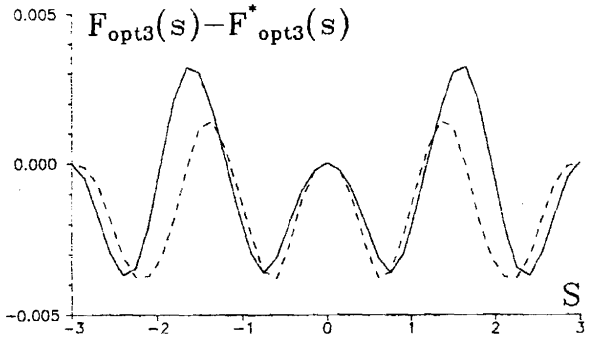

Figure 11: A deviation function $F_{opt3}(s) - F^*_{opt3}(s)$. The solid line shows the difference between upper surfaces and the dashed line corresponds to the lower surfaces.

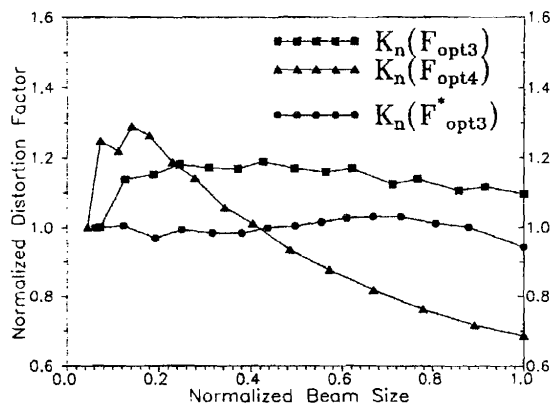

Figure 12: A normalized distortion factors for $F_{opt3}(s)$ (rectangulars), for $F_{opt4}(s)$ (triangles) and for $F^*_{opt3}(s)$ (circles). The distortion factor was calculated for all $l^{object} = l^{image} = 0.5$.

References

[1] L.C.Martin, Technical Optics, vol. 2, London, Sir Isaac Pitman & Sons, Ltd.

[2] M.M.Rusinov, Technical Optics, MASHGIS Publishers, Moscow-Leningrad (1961), in Russian.

[3] Huygens, Traité de la Lumiére, 1690.

[4] L.G.Vorobiev and R.W.Müller, GSI-96-06 Report, Darmstadt, (1996).

[5] L.G.Vorobiev and D.G.Koshkarev, Preprint ITEP-9, Moscow (1992).

[6] D.G.Koshkarev and L.G.Vorobiev, Nuclear Instruments and Methods, Section A, **336**, (1993), pp. 291-300.

[7] G.A.Korn and T.M.Korn, "Mathematical Handbook", McGraw-Hill (1968).

Л.Г.Воробьев

Метод расчета асферических линз,применимый к оптике заряженных частиц и световых объектов.

Подписано к печати 07.04.97 Формат 60x90 I/I6 Офсетн.печ.
Усл.-печ.л.I,0 Уч.-изд.л.0,7. Тираж 9I экз. Заказ I7.
Индекс 3649

Отпечатано в ИТЭФ, II7259, Москва, Б.Черемушкинская, 25